PI3Kδ as a Novel Therapeutic Target in Pathological Angiogenesis

Wenyi Wu,[1,2] Guohong Zhou,[2,3] Haote Han,[2] Xionggao Huang,[2,4] Heng Jiang,[2,5] Shizuo Mukai,[6] Andrius Kazlauskas,[7] Jing Cui,[8] Joanne Aiko Matsubara,[8] Bart Vanhaesebroeck,[9] Xiaobo Xia,[1] Jiantao Wang,[10] and Hetian Lei[10]

Diabetes 2020;69:736–748 | https://doi.org/10.2337/db19-0713

Diabetic retinopathy is the most common microvascular complication of diabetes, and in the advanced diabetic retinopathy appear vitreal fibrovascular membranes that consist of a variety of cells, including vascular endothelial cells (ECs). New therapeutic approaches for this diabetic complication are urgently needed. Here, we report that in cultured human retinal microvascular ECs, high glucose induced expression of p110δ, which was also expressed in ECs of fibrovascular membranes from patients with diabetes. This catalytic subunit of a receptor-regulated PI3K isoform δ is known to be highly enriched in leukocytes. Using genetic and pharmacological approaches, we show that p110δ activity in cultured ECs controls Akt activation, cell proliferation, migration, and tube formation induced by vascular endothelial growth factor, basic fibroblast growth factor, and epidermal growth factor. Using a mouse model of oxygen-induced retinopathy, p110δ inactivation was found to attenuate pathological retinal angiogenesis. p110δ inhibitors have been approved for use in human B-cell malignancies. Our data suggest that antagonizing p110δ constitutes a previously unappreciated therapeutic opportunity for diabetic retinopathy.

Diabetic retinopathy is the most common of microvascular complications of diabetes and a leading cause of blindness (1). Pathological angiogenesis is associated with proliferative diabetic retinopathy (PDR), an advanced stage of diabetic retinopathy (2). Proangiogenic molecules, including basic fibroblast growth factor (bFGF) (3), epidermal growth factor (EGF) (4), and vascular endothelial growth factor (VEGF) (5), promote proliferation and migration of vascular endothelial cells (ECs), initiating pathological angiogenesis. Currently, available treatments of diabetic retinopathy include neutralizing VEGF in the vitreous using either antibodies against VEGF (ranibizumab, bevacizumab) or a recombinant fusion protein consisting of an antibody Fc fragment fused to the extracellular domains of VEGF receptor 1 and 2 (aflibercept) (6–8). These anti-VEGF agents reduce neovascular growth and lessen vascular leakage; however, resistance to these drugs or recurrence of disease is observed in a significant number of patients with PDR (1,9), and new therapeutic approaches are urgently needed.

During the process of angiogenesis, a series of proangiogenic intracellular signaling cascades are rapidly activated, including the phosphoinositide 3-kinase (PI3K)/Akt pathway (10,11). PI3Ks have been divided into three classes (I, II, and III) on the basis of their structural features and lipid substrate preference (10). Class IA PI3Ks are composed of a p110 catalytic subunit (p110α, p110β or p110δ) bound to one of five p85 regulatory subunits (12). Whereas p110α and p110β are ubiquitously expressed, p110δ is mainly expressed in white blood cells (13) and controls immune

[1]Department of Ophthalmology, Xiangya Hospital, Central South University, Changsha, China
[2]Schepens Eye Research Institute of Massachusetts Eye and Ear and Department of Ophthalmology, Harvard Medical School, Boston, MA
[3]Shanxi Eye Hospital, Taiyuan, China
[4]Department of Ophthalmology, the First Affiliated Hospital of Hainan Medical University, Haikou, China
[5]Department of Ophthalmology, Second Xiangya Hospital, Central South University, Changsha, China
[6]Massachusetts Eye and Ear, Department of Ophthalmology, Harvard Medical School, Boston, MA
[7]Department of Ophthalmology and Visual Sciences and Department of Physiology and Biophysics, University of Illinois at Chicago, Chicago, IL
[8]The University of British Columbia, Vancouver, British Columbia, Canada
[9]Cancer Institute, University College London, London, U.K.
[10]Shenzhen Eye Hospital, Shenzhen Eye Institute, Shenzhen, China
Corresponding author: Hetian Lei, leihetian18@hotmail.com

Received 20 July 2019 and accepted 25 December 2019
This article contains Supplementary Data online at https://diabetes.diabetesjournals.org/lookup/suppl/doi:10.2337/db19-0713/-/DC1.

functions (14–16). The main regulator of angiogenesis has been reported to be p110α (17), with a modest role of p110β (18). A role for p110δ in angiogenesis has not been reported. Small-molecule inhibitors of p110δ are being explored clinically as pharmacological treatments for inflammatory disease and cancer (19), and three compounds that share the ability to target p110δ have recently been approved for use in human B-cell malignancies (12,20).

However, while expression of p110δ is known to be expressed at low levels in other cells than leukocytes, including fibroblast-like cells (21) and ECs (22), and become further induced by tumor necrosis factor-α (TNF-α) in ECs (22), its role in these tissue contexts is unknown. In the current study, we uncover functional roles of p110δ activity in cultured ECs and in pathological angiogenesis in a mouse model of oxygen-induced ischemic retinopathy (OIR).

RESEARCH DESIGN AND METHODS

Major Reagents

VEGF-A (further referred to as VEGF) (catalog number [Cat.] 293-VE-010), bFGF (Cat. 233-FB), EGF (Cat. 236-EG), and PDGF-A (Cat. 221-AA) were purchased from R&D Systems (Minneapolis, MN). Antibodies against p110α (Cat. 4249), p110β (Cat. 3011), p110δ (Cat. 34050), Akt (Cat. 9272), phospho-Akt (S473) (Cat. 4058), CD31 (Cat. 3528), and vascular endothelial-cadherin (Cat. 2500) were purchased from Cell Signaling Technology (Danvers, MA). L-Glucose (Cat. G5500) and D-glucose (Cat. G7021) were purchased from Sigma (St. Louis, MO); idelalisib (Cat. CAL101) was purchased from APExBIO (Houston, TX). The primary antibody against β-actin (Cat. sc-47778) and secondary antibodies of horseradish peroxidase (HRP)–conjugated goat anti-rabbit IgG (Cat. sc-2004) and anti-mouse IgG (Cat. sc-2005) were purchased from Santa Cruz Biotechnology (Dalla, TX). Enhanced chemiluminescence substrate for detection of HRP (Cat. 34580) was obtained from Thermo Fisher Scientific (Waltham, MA). Alexa Fluor 594–conjugated mouse endothelial-specific isolectin B4 (IB4) (Cat.112413) was purchased from Life Technology (Grand Island, NY). High-fidelity herculase II DNA polymerases (Cat. 600677) were from Agilent Technologies (Santa Clara, CA).

DNA Constructs

The three 20-nucleotide (nt) target DNA sequences preceding a 5′-NGG protospacer-adjacent motif (PAM) sequence at exon 4 in the human genomic *PIK3CD* locus (NG_023434) (23) were selected for generating single-guide RNA (sgRNA) for SpCas9 targets. The control sgRNA sequence (5′-TGCGAATACGCCCACGCGATGGG-3′) was designed to target the *lacZ* gene from *Escherichia coli* (24). The lenti-CRISPR v2 vector (25) was purchased from Addgene (23) (Cat. 52961; Cambridge, MA).

To express SpGuides in the targeted cells, the top oligos 5′-CACCG-20nt (target *PI3KCD* DNA sequences PK2 [AGAGCGGCTCATACTGGGCG], PK3 [TGTGGAAGAGCGG CTCATAC], PK4 [TCTTCACGCGGTCGCCCTCA], or the *lacZ* sgRNA sequence)-3′ and bottom oligos 5′-AAAC-20nt (20nt: complementary target *PI3KCD* DNA sequences or *lacZ* sgRNA sequence)-C-3′ were annealed and cloned into the lenti-CRISPR v2 vector, respectively. All clones were confirmed by Sanger DNA sequencing using a primer 5′-GGACTATCATATGCTTACCG-3′ from a sequence of U6 promoter, which drives expression of sgRNAs. DNA synthesis and sequencing were performed by the Massachusetts General Hospital DNA Core Facility (Cambridge, MA).

Cell Culture

Three vials of human primary retinal microvascular ECs (HRECs) isolated from three different donors were purchased from Cell Systems (Cat. ACBRI181; Kirkland, WA) and cultured in Endothelial Growth Medium (EGM) 2 (5 mmol/L D-glucose) (Cat. 213KS-500; Cell Applications, San Diego, CA) or EGM in addition to L-glucose (25 mmol/L) or D-glucose (25 mmol/L) for 1 week (26). HRECs were used from passages 6–10 for following experiments, and their tissue culture dishes were precoated with gelatin-based coating solution (Cat. 6950; Cell Biologics, Chicago, IL). The media were changed every other day. All cells were cultured at 37°C in a humidified 5% CO_2 atmosphere (23,27).

Porcine aortic ECs (PAECs) (26) overexpressing platelet-derived growth factor receptor-α (PDGFR-α) were cultured in DMEM/F12 medium supplemented with 10% FBS (Cat. S11150; Bio-Techne, Minneapolis, MN). Human primary lymphatic ECs (HLECs) were purchased from Cell Biologics (Cat. H6092), and human umbilical vein ECs (HUVECs) were purchased from Cell Applications (Cat. 200-05f). These primary ECs were cultured in EGM-2. Mouse cone photoreceptor cells (661W) were obtained by material transfer agreement from the University of Houston (Houston, TX), RAW264.7 mouse macrophages (Cat. TIB-71) were purchased from ATCC (Manassas, VA) (28), rabbit conjunctival fibroblasts (RCFs) were a gift from A.K. (29), and human embryonic kidney (HEK) 293T cells (HEK 293 containing SV40 T antigen) were from the Dana-Farber Cancer Institute/Harvard Medical School (Boston, MA). Cells of 661W, RAW264.7, RCFs, and HEK 293T were cultured in high-glucose (4.5 g/L) DMEM supplemented with 10% FBS. The medium used to harvest the lentiviral supernatant from 293T cells was high-glucose DMEM supplemented with 20% FBS. All cells were cultured at 37°C in a humidified 5% CO_2 atmosphere (23,27).

Quantitative PCR

HRECs were plated into six-well plates at a density of 1×10^5 cells/well and treated with EGM in addition to L-glucose (25 mmol/L) or D-glucose (25 mmol/L) for 1 week. Total RNA was extracted using the RNeasy Plus Mini Kit (Cat. 74104; QIAGEN, Germantown, MD). The levels of *PIK3CD* mRNA were normalized to the levels of human hypoxanthine phosphoribosyltransferase 1 (*hHPRT1*) mRNA. Primers of quantitative PCR synthesized by Integrated DNA Technology (Coralville, IA) were forward: 5′-GAATCAGAGCGT

TGTGGTTG-3′, reverse: 5′–CAGAATTGGCACATCTTGGC- 3′, for *PIK3CD* and forward: 5′-CCTGGCGTCGTGATTAGT GAT-3′, reverse: 5′-AGACGTTCAGTCCTGTCCATAA-3′, for the housekeeping gene *hHPRT1* (30).

Western Blot Analysis

HRECs at 90% confluence in a 24-well plate were deprived of serum and growth factors for continuous incubation for 8 h, and then some of these cells were treated as desired. After washing twice with PBS, cells were lysed. The clarified lysates were subjected to Western blot analysis using the appropriate antibodies. Experiments were repeated at least three times. Signal intensity was determined by densitometry using National Institutes of Health ImageJ software (https://imagej.nih.gov/ij) (23).

MTT Assay

The toxicity of idelalisib on cell viability was assessed using the 3-(4,5-dimethylthiazol-2-yl)-2,5-diphenyl-2H-tetrazolium bromide (MTT) assay (Cat. M2128; Sigma) as described previously (31). Briefly, HRECs were seeded into 96-well plates and incubated for 24 h before exposure to a range of concentrations (0, 5, 10, 15, 20, 25, 30, 35, and 40 μmol/L) of test articles dissolved in DMSO in 5% FBS-supplemented medium for 24–72 h. Each condition was tested with six replicates, and all assays were performed in triplicate (31).

Cell Proliferation Assay

HRECs were seeded into 24-well plates at a density of 30,000 cells/well in an EGM kit. After attaching the plates, the cells were starved of growth factors for 8 h and then treated with idelalisib (10 μmol/L) with or without VEGF, bFGF, and EGF (20 ng/mL each). The treatment was repeated daily. After 48 h, the cells were trypsin detached and then counted in a hemocytometer under a light microscope (23).

Wound Healing Assay

The wound healing assay was performed as previously described (23) with minor modifications. Once HRECs reached confluence in 48-well plates, they were starved for growth factors for 8 h. After the cell monolayer was scraped with a 200-μL sterile pipette tip, the cells were washed twice with PBS to remove detached cells. The cells were treated with idelalisib (10 μmol/L) supplemented with or without VEGF, bFGF, and EGF (20 ng/mL). The wound was photographed at 0 and 18 h post-wounding under a microscope (23).

Tube Formation Assay

This assay was performed as previously described (23) with minor modifications. Briefly, the collagen gel mixture was added to a 96-well plate (70 μL/well), which was then incubated for ~60 min at 37°C to let the collagen gel polymerize. After polymerization, HRECs (4.5×10^4) were seeded in each well with their cultured medium and maintained in a 37°C incubator. This day was considered day 1. On day 2, the medium was removed, and 30 μL of the gel mixture was added to each well. After incubation for ~60 min at 37°C, the collagen gel was polymerized, and the medium (100 μL) (endothelial basal medium supplemented with 0.5% horse serum, 0.1% bovine brain extract supplemented with VEGF, bFGF, and EGF [20 ng/mL]) in addition to idelalisib (10 μmol/L). On day 3, the gel was photographed using the EVOS FL Auto microscope (23).

Breeding and Genotyping

Six-week-old heterozygous $p110\delta^{D910A/D910A}$ C57BL/6J (B6) mice were purchased from Charles River Laboratories (Boston, MA) and used for breeding to generate wild-type (WT), heterozygous, and mutant $p110\delta^{D910A/D910A}$ pups. Genomic DNA was isolated from postnatal day (P) 12 mice by boiling tail tips in 100 μL lysis buffer (0.125 mol/L NaOH, 2 mmol/L EDTA) for 25 min, followed by the addition of 100 μL neutralizing buffer (40 mmol/L Tris HCl, pH 8.0). The supernatant after spin was used for PCR using the P28 primer (forward: 5′-CCTGCACAGAAATGC ACTTCC-3′, reverse: 5′-AACGAAGCTCTCAGAGAAAGCTG-3′). The expected PCR fragments from mutant and WT mice are 500 and 332 base pairs, respectively (32).

Mouse Model of OIR

This experiment was performed as described previously (33,34). Briefly, B6 litters on P7 were exposed to 75% oxygen until P12 in an oxygen chamber (BioSpherix, Parish, NY). At P12, intravitreous injections were performed under a microsurgical microscope. One microliter of idelalisib (final vitreal concentration 10 μmol/L) or its vehicle (0.1% DMSO) on the basis of a 5-μL vitreous volume was injected. After the intravitreal injection, the eyes were treated with a triple antibiotic (Neo/Poly/Bac) ointment and kept in room air (21% oxygen). At P17, the mice were euthanized, and retinas were carefully removed for Western blot analysis or fixed in 3.7% paraformaldehyde. Mice <6 g of total body weight were excluded from the experiments. Retinal whole mounts were stained overnight at 4°C with the murine-specific EC marker IB4-Alexa Fluor 594 (red) (33). The images were taken with an EVOS FL Auto microscope.

ELISA

This experiment was performed by following the instructions of a Quantikine Mouse VEGF ELISA Kit (Cat. MMV00; R&D Systems). Briefly, clarified vitreous (5 μL) from each eye from P17 mice with or without experiencing OIR was diluted with PBS to 50 μL, which was added into each well. In addition, 50 μL standard was added to each well, and incubated at room temperature for 2 h. Then, after the wells were washed with wash buffer for five times, 100 μL conjugate from the kit was added to each well and incubated at room temperature for 2 h. After wash for five times, 100 μL substrate solution was added to each well and incubated for 30 min. Then, 100 μL of stop solution was added into each well. Finally, the plate was read at 450 nm within 30 min (35).

Examination of Idelalisib Toxicity in Mouse Eyes

At P12, five pups were anesthetized and underwent intravitreal injections as described above. A single dose of 1 μL of 50 μmol/L idelalisib stock (dissolved in 0.1% DMSO) was injected. Control injections were performed with 1 μL of the 0.1% DMSO vehicle. On the basis of the notion that the mouse vitreous volume is 5 μL, this is expected to give rise to an initial final vitreal

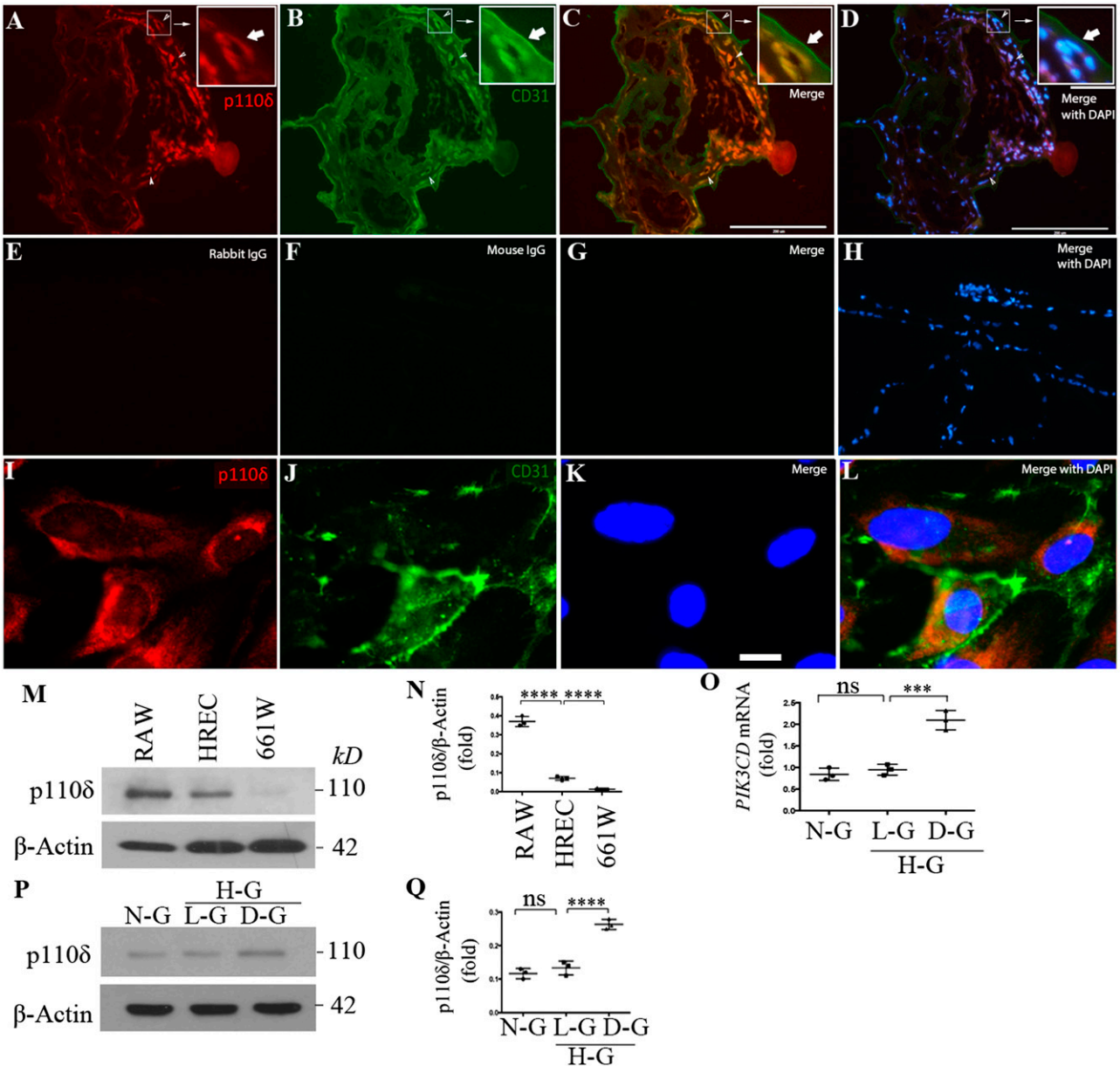

Figure 1—High glucose induced p110δ expression in vascular ECs. *A–H*: Slides of FVMs from patients with PDR were subjected to immunofluorescence analysis using antibodies against p110δ and CD31 (*A–D*) or control antibodies (rabbit and mouse) IgG (*E–H*). Red and green signals indicate expression of p110δ and CD31, respectively, compared with the negative nonimmune IgG-stained control. Blue signals are from nucleus staining with DAPI. This is a representative of three independent experiments using different sample sources (FVMs from three patients with PDR). The images were taken under immunofluorescence microscope. Scale bars = 200 μm. *I–L*: HRECs at passage 6 in a slide chamber were subjected to immunofluorescence analysis using antibodies against p110δ and CD31 as performed in *A–H*. Scale bar = 20 μm. *M* and *N*: Lysates of RAW264.7 (RAW), HRECs, and 661W cells were subjected to Western blot analysis using the indicated antibodies. The intensity of the p110δ bands was first normalized to that of the corresponding β-actin bands. Data in *N* are mean ± SD of three independent experiments (folds). $^{****}P < 0.001$ between two compared groups using one-way ANOVA followed by a Tukey post hoc test. *O–Q*: HRECs exposed to normal D-glucose (N-G, 5 mmol/L), L-glucose (L-G, 5 mmol/L D-glucose + 25 mmol/L L-glucose), and high D-glucose (D-G, 5 mmol/L original D-glucose + 25 mmol/L additional D-glucose) for 1 week were subjected to quantitative PCR and Western blot for analysis of mRNA and protein expression. The intensity quantitation of protein expression was performed in *P* and *Q*. Data in *O* and *Q* are mean ± SD of three independent experiments (folds). $^{***}P < 0.001$, $^{****}P < 0.0001$ by one-way ANOVA followed by the Tukey post hoc test. H-G, high glucose.

concentration of 9–10 μmol/L, which is expected to be further diluted over time.

Four weeks later, electroretinography (ERG) (by light/dark adaptation, using a Diagnosys ColorDome containing an interior stimulator), optical coherence tomography (OCT), and fluorescein fundus angiography (FFA) were performed as described previously (34). After the mice were euthanized, representative eyeballs were carefully removed, fixed in 3.7% paraformaldehyde, and embedded in paraffin for histopathological analysis.

All animal experiments followed the guidelines of the Association for Research in Vision and Ophthalmology Statement for the Use of Animals in Ophthalmic and Vision Research. Investigators who conducted the analysis were masked to the treatment groups. All the mice were cared for by following the protocol approved by the institutional animal care and use committee at Schepens Eye Research Institute.

Immunofluorescence

Embedded frozen fibrovascular membranes (FVMs) from patients with PDR were prepared as described previously (36). An ethical approval was obtained before the initiation of this project from the Vancouver Hospital and The University of British Columbia Clinical Research Ethics Board. The University of British Columbia Clinical Research Ethics Board policies comply with the Tri Council Policy and the Good Clinical Practice Guidelines, which have their origins in the ethical principles of the Declaration of Helsinki. Written informed consent was obtained from patients.

FVMs on slides or cultured HRECs were fixed in 3.7% formaldehyde/PBS for 10 min. Subsequently, the sections or cells were preincubated with 5% normal goat serum in 0.3% Triton X-100/PBS for 20 min and incubated with primary antibodies against p110δ (1:100 dilution) (Cat. ab2003372; Abcam, Cambridge, MA) for 1 h or a normal rabbit IgG. After three washes with PBS, the tissues and sections were incubated with fluorescently labeled secondary antibody DyLight 549 (Cat. DI-1549; Vector Laboratories, Burlingame, CA) (1:300 dilution in blocking buffer) for 30 min. Following three washes with PBS, the slides were mounted with a mount medium containing DAPI (Cat. H-1200; Vector Laboratories) and photographed under a fluorescence microscope (26,37,38).

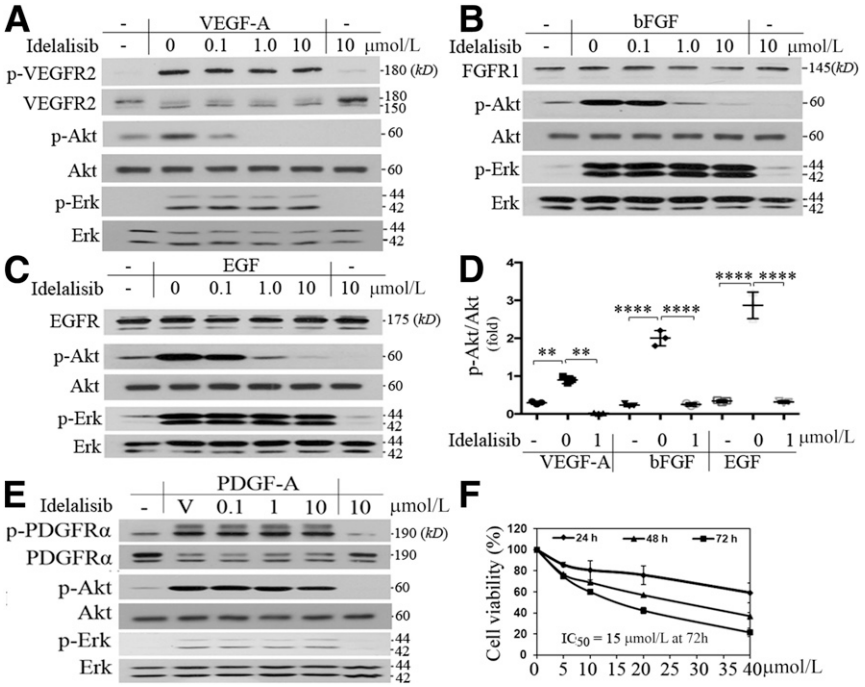

Figure 2— Inhibition of PI3Kδ prevents Akt activation induced by VEGF, bFGF, or EGF. *A–D*: When HRECs reached ∼90% confluence, the cultured medium was replaced with the endothelial basal medium without growth factors and continuously cultured for 8 h. Then, these cells were treated with idelalisib at the indicated concentrations or its vehicle in addition to VEGF-A (*A*), bFGF (*B*), or EGF (*C*) (10 ng/mL). After this treatment lasted for 15 min, the cells were lysed. Their lysates were subjected to a Western blot analysis using the indicated antibodies. A representative of three independent experiments is shown. *E*: Serum-deprived PAECs, which overexpressed PDGFR-α, were treated with idelalisib at the indicated concentrations or its vehicle in addition to PDGF-A (10 ng/mL) for 15 min. Their lysates were subjected to Western blot analysis using the indicated antibodies; this is representative of three independent experiments. *F*: HRECs treated with idelalisib at the indicated concentrations and time courses were subjected to an MTT assay. IC_{50} of idelalisib to HRECs was 15 μmol/L at 72 h. Data in *D* are mean ± SD of three independent experiments (folds). $^{**}P < 0.01$, $^{****}P < 0.0001$ by one-way ANOVA followed by the Tukey post hoc test. V, vehicle (0.1% DMSO).

Flow Cytometry

Cultured HRECs were harvested and incubated with antibodies against vascular endothelial-cadherin, CD31, or nonimmune IgG for 2 h at room temperature. After washing twice with 0.3% Triton X-100/PBS, the cells were incubated with fluorescence-labeled secondary antibodies for 1 h at room temperature. After additional triple washes with 0.3% Triton X-100/PBS, the cells were subjected to FACS analysis as described previously (23).

Statistics

The data from three independent experiments were analyzed using an unpaired *t* test between two groups and one-way ANOVA followed by Tukey post hoc test among more than two groups. For animal experiments, the data from at least six mice were used for the statistical analysis. All data were analyzed using a masked procedure. $P < 0.05$ was considered statistically significant.

Data and Resource Availability

The data sets and resource generated and/or analyzed during the current study are available from the corresponding author upon reasonable request.

RESULTS

p110δ Is Expressed in Vascular ECs

The tissue distribution of p110δ is more restricted than that of the ubiquitously expressed other PI3K isoforms p110α and p110β (13). Previous studies showed that p110δ is primarily expressed in leukocytes, but it is also found at lower levels in some nonleukocyte cell types, such as ECs (22,39). As TNF-α induces p110δ expression in ECs (22) and inflammation plays an important role in diabetic retinopathy (40,41), we examined whether p110δ was expressed in ECs in FVMs from patients with PDR. Immunofluorescence revealed that p110δ was indeed expressed in ECs of FVMs (Fig. 1*A*–*H*); in addition, we found that p110δ was expressed in cultured HRECs (Fig. 1*I*–*L* and Supplementary Fig. 1) and that its expressional level was lower than that in mouse macrophages but much higher than that in cultured mouse cone cells (661W) (Fig. 1*M* and *N*). Specifically, p110δ was expressed at 6.1 ± 0.7- and 22.4 ± 1.1-fold more in cultured HRECs and RAW264.7 mouse macrophages, respectively, than that in cultured 661W cells (Fig. 1*N*). Importantly, we discovered that high glucose (5 mmol/L + 25 mmol/L) for 1 week enhanced approximately twofold the expression of p110δ in HRECs in mRNA (Fig. 1*O*) and protein (Fig. 1*P* and *Q*). Additionally, expression of p110δ was detected in other vascular ECs, including HUVECs, PAECs, and HLECs (Supplementary Fig. 2). In contrast, the expression level of p110δ was very low in RCFs (42) and mouse 661W cone photoreceptor cells (28) (Fig. 1*M* and *N* and Supplementary Fig. 2). These results demonstrate that p110δ is expressed in eye-related pathological and cultured ECs and that high glucose promotes its expression in cultured ECs, suggesting that p110δ plays a biological role in ECs.

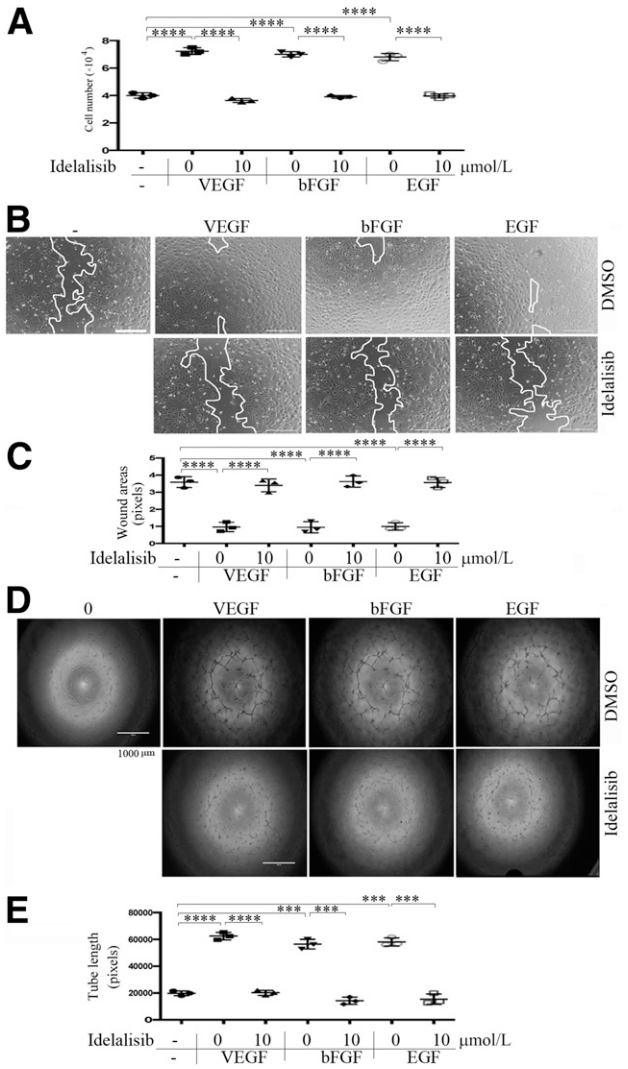

Figure 3—Inhibition of PI3Kδ inhibits cell proliferation, migration, and tube formation induced by VEGF, bFGF, or EGF. *A*: HRECs were seeded into 24-well plates at a density of 30,000 cells/well in EGM. After attaching the plates, the cells were starved of growth factors for 8 h and then treated with idelalisib (10 μmol/L), or its vehicle, in addition to VEGF, bFGF, or EGF (20 ng/mL). After 24 h, the cells were trypsin detached and then counted in a hemocytometer under a light microscope. *B* and *C*: When HRECs reached confluence in 48-well plates and starved of growth factors for 8 h, a wound was created by scraping the cell monolayer with a sterile pipette tip. The cells were washed twice to remove detached cells and then treated with idelalisib (10 μmol/L), or its vehicle, in addition to VEGF, bFGF, or EGF (20 ng/mL). At 18 h post-wounding, the wound was photographed under a microscope. Scale bar = 400 μm. *D* and *E*: After polymerization of the collagen gel, HRECs (4.0×10^4) were seeded in each well in the culture medium overnight. After addition of a second layer of gel, cells were treated with idelalisib (10 μmol/L), or its vehicle, in addition to VEGF, bFGF, or EGF (20 ng/mL). Six hours later, each well was photographed under a microscope. Data in *A*, *C*, and *E* are mean ± SD of three independent experiments. ***$P <$ 0.001, ****$P < 0.0001$ by one-way ANOVA followed by the Tukey post hoc test.

p110δ Inhibition Prevents Akt Activation and Biological Responses Induced by VEGF, bFGF, and EGF

PI3K activation is necessary for VEGF-induced proliferation, migration, and survival of cultured ECs (43). ECs express multiple PI3K isoforms, and work from other groups has indicated that not all isoforms are required for the VEGF-driven responses (17). For instance, inactivation of p110α does not block VEGF-induced proliferation and survival of vascular ECs (17). In contrast, we found that the p110δ-selective inhibitor idelalisib at 1 μmol/L for 15 min completely prevented VEGF-induced Akt activation (as measured by its phosphorylation on serine 473) (Fig. 2*A* and *D*). This was also observed for Akt activation induced by bFGF (Fig. 2*B* and *D*) or EGF (Fig. 2*C* and *D*). In contrast, growth factor–stimulated phosphorylation of Erk (p-E202/p-Y204) was not affected (Fig. 2*A*–*C*); in addition, idelalisib at 10 μmol/L only modestly inhibited PDGF-A–induced activation of Akt in PAECs that overexpress PDGFR-α (Fig. 2*E*), suggesting that different RTKs preferentially select different PI3K isoforms for transducing signaling to Akt and that the 10 μmol/L concentration of idelalisib is selective. This assumption was also supported by a cell viability assay, which indicated that idelalisib, even at higher doses, was within the nontoxic range (Fig. 2*F*). These data demonstrate that p110δ regulates a subset of RTK-triggered signaling pathways in HRECs, including Akt, known to play a central role in angiogenesis (44,45). In line with these observations, idelalisib was also found to blunt VEGF-, bFGF-, or EGF-promoted EC proliferation (Fig. 3*A*), migration (Fig. 3*B* and *C*), and tube formation (Fig. 3*D* and *E*).

p110δ Depletion Attenuates Akt Activation, Proliferation, Migration, and Tube Formation of HRECs

To complement and substantiate our data from the pharmacological approach using idelalisib, we next depleted p110δ in HRECs using CRISPR/Cas9 technology (23,24). As shown in Fig. 4*A*–*E* and Supplementary Fig. 3, the CRISPR/Cas9 system guided by PK2-based sgRNA targeting *PIK3CD* resulted in DNA insertion and deletion in the expected genomic site, leading to depletion of p110δ expression, without affecting expression of p110α and p110β (Fig. 4*A*–*C*). Importantly, this p110δ depletion attenuated Akt activation induced by VEGF (Fig. 4*D*–*F*),

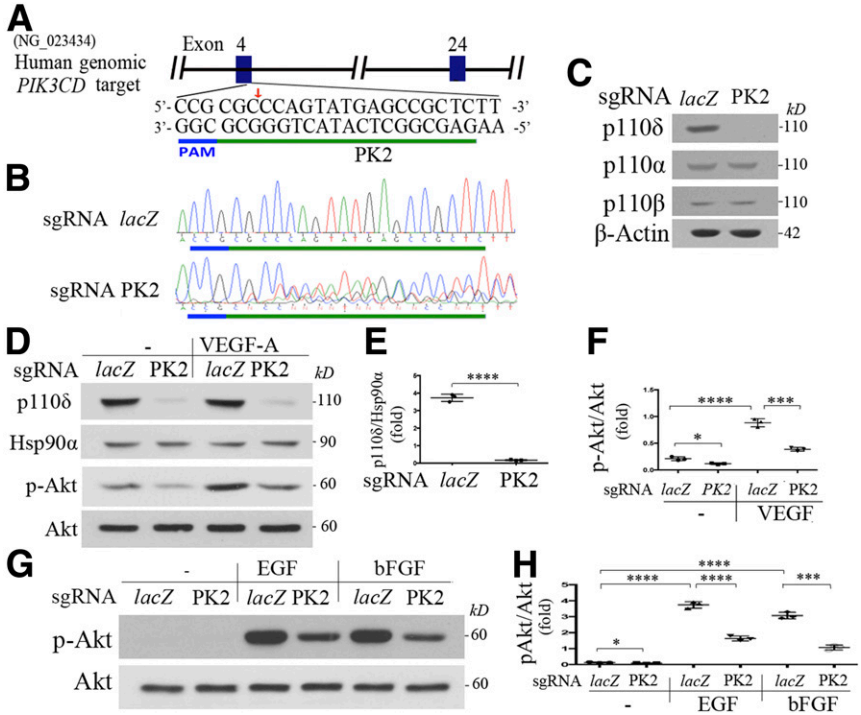

Figure 4— Depletion of p110δ attenuates Akt activation induced by VEGF, bFGF, or EGF. *A*: Schematic of the human genomic *PIK3CD* locus. One target for generating its sgRNA was selected at the human genomic *PIK3CD* exon 4 and named as PK2 (green line). The PAM sequences are marked in a blue line. *B*: Genomic DNA isolated from HRECs with CRISPR/Cas9 targeting to *PIK3CD* by sgRNA-PK2 or control by sgRNA-*lacZ* was used to PCR amplify the DNA fragments around the sgRNA-PK2 protospacer with primers P24F1 (5′-GGGAGGTTTGGACCCC CAG-3′) and P24R1 (5′-ACCTTTGCCGATGAGGAGGC-3′) for Sanger DNA sequencing. *C*: Lysates of HRECs expressing sgRNA-*lacZ* or PK2/Cas9 were subjected to Western blot analysis using the indicated antibodies. This is representative of three independent experiments. *D–H*: The characterized HRECs in *B* were cultured to 90% confluence and then starved of growth factors for 8 h. Subsequently, these cells were treated with VEGF, bFGF, and EGF (10 ng/mL) for 15 min, and their clarified lysates were subjected to Western blot analysis using the indicated antibodies. A representative of three independent experiments is shown. The intensity of the bands from three experiments was quantified as dot plots. Data in *F* and *H* are mean ± SD of three independent experiments. $^*P < 0.05$, $^{***}P < 0.001$, $^{****}P < 0.0001$ by one-way ANOVA followed by the Tukey post hoc test.

bFGF, and EGF (Fig. 4*G* and *H*) and diminished cell proliferation (Fig. 5*A* and *B*), migration (Fig. 5*C*), and tube formation (Fig. 5*D*) in these cells. Of note, idelalisib at 10 μmol/L did not further inhibit cell proliferation in p110δ-depleted cells (Fig. 5*B*), indicating that both idelalisib and PK2-based sgRNA are specific for p110δ. These results demonstrate that p110δ plays an essential role in Akt activation and cellular responses induced by these growth factors in HRECs.

Genetic Inactivation of p110δ in Mice Reduces Akt Activation and Abnormal Angiogenesis in a Mouse Model of OIR

To investigate the impact of p110δ on pathological angiogenesis, mice with genetic inactivation of p110δ (32) were subjected to a model of OIR (34). In the p110δ-inactive mice, their endogenous p110δ was replaced through germline knockin mutation with a catalytically inactive form of p110δ called $p110\delta^{D910A}$ (32) (Supplementary Fig. 4), and their p110δ lipid kinase activity is fully ablated, with no changes in the kinase activities of p110α and p110β (32).

In this mouse model of OIR, P7 mouse pups with nursing mothers are subjected to hyperoxia (75% oxygen) for 5 days, which prevents retinal vessel growth and leads to significant vessel loss in the central retina. At P12, mice were returned to room air. The switch from high oxygen to room air creates a relatively hypoxic condition that triggers both normal vessel regrowth in the avascular area of central retina and abnormal retinal angiogenesis toward the normally avascular vitreous cavity to form unorganized, small-caliber vessels, termed preretinal tufts, that reach a maximum at P17 (33,34). These preretinal tufts resemble the pathological neovascularization seen in human PDR. This OIR model has helped to lay the foundation for the present clinical application of anti-VEGF therapies in patients with PDR (46–48).

Thus, OIR was induced in homozygous $p110\delta^{D910A}$ mice (further referred to as $p110\delta^{D910A/D910A}$) and their WT littermates by the techniques described above. At P17, the whole-mount retinas from the euthanized pups were stained with IB4, a mouse endothelial marker. The IB4 staining revealed a significant reduction in the area of preretinal tufts (pathological angiogenesis) in the eyes of $p110\delta^{D910A/D910A}$ mice compared with those of littermate WT mice, with no significant difference in the areas of vaso-obliteration between the two mouse lines (Fig. 6*A*–*C*). Western blot analysis showed that there was significantly less activated Akt in the retinas from P17 $p110\delta^{D910A/D910A}$ mice compared with those from the P17 WT mice (Fig. 6*D*). Furthermore, ELISA indicated that there was less VEGF in the vitreous from the P17 $p110\delta^{D910A/D910A}$ mice than that from the P17 WT mice experiencing OIR (Supplementary Fig. 5). These data demonstrate that genetic inactivation of p110δ decreases hypoxia-induced Akt activation and inhibits pathological angiogenesis but not central retinal avascular area to form neovascularization in this OIR mouse model.

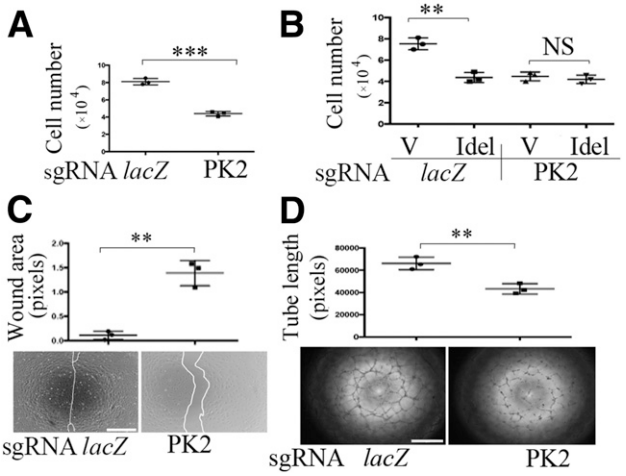

Figure 5—Depletion of p110δ attenuates cell proliferation, migration, and tube formation. *A* and *B*: HRECs expressing *lacZ* or PK2-sgRNA/Cas9 were seeded into 24-well plates at a density of 30,000 cells/well in an EGM kit with or without treatment with idelalisib (Idel) (10 μmol/L). After 24 h, the cells were trypsin detached and counted in a hemocytometer under a light microscope. *C*: When HRECs reached 90% confluence in 48-well plates, a wound was created by scraping the cell monolayer with a 200-μL sterile pipette tip. At 18 h post-wounding, the wound was photographed under a microscope. Shown is a representative of three independent experiments. Scale bar = 400 μm. *D*: A collagen gel mixture was added to a 96-well plate. After polymerization, HRECs (4.0×10^4) were seeded in each well, with their culture medium maintained in a 37°C incubator. The next day, the top gel was added. Six hours later, each well was photographed under a microscope. Shown is a representative of three independent experiments. Scale bar = 400 μm. Data are mean ± SD of three independent experiments. $^{**}P < 0.01$, $^{***}P < 0.001$ in *A*, *C*, and *D* between the two compared groups by unpaired *t* test and in *B* by one-way ANOVA followed by the Tukey post hoc test. V, vehicle.

Idelalisib Prevents Hypoxia-Induced Akt Activation and Abnormal Retinal Angiogenesis in a Mouse Model of OIR

To explore the impact of idelalisib on angiogenesis in vivo, we used a mouse model of OIR in the eye because the preretinal tufts formed in this model resemble the pathological neovascularization seen in human PDR (34). We first tested the effects of an intravitreal injection of a single dose of idelalisib into P12 mice at a vitreal concentration of 8–10 μmol/L (a dose that did not cause obvious damage to cultured HRECs) (Fig. 2*F*) followed by examination of the mouse eyes 30 days later. This was done by ERG and FFA to evaluate retinal function and by OCT and histological analysis to evaluate retinal structure (Fig. 7). These four assays revealed no functional or structural damage to the retina 30 days after a single injection of idelalisib.

We next examined the impact of idelalisib on pathological angiogenesis in the mouse model of OIR (33,34). In this model as described above, at P12, when mice were returned to room air, idelalisib (initial vitreal concentration of a single dose of 8–10 μmol/L) or its vehicle (DMSO, 0.1% initial concentration) was injected into the vitreous.

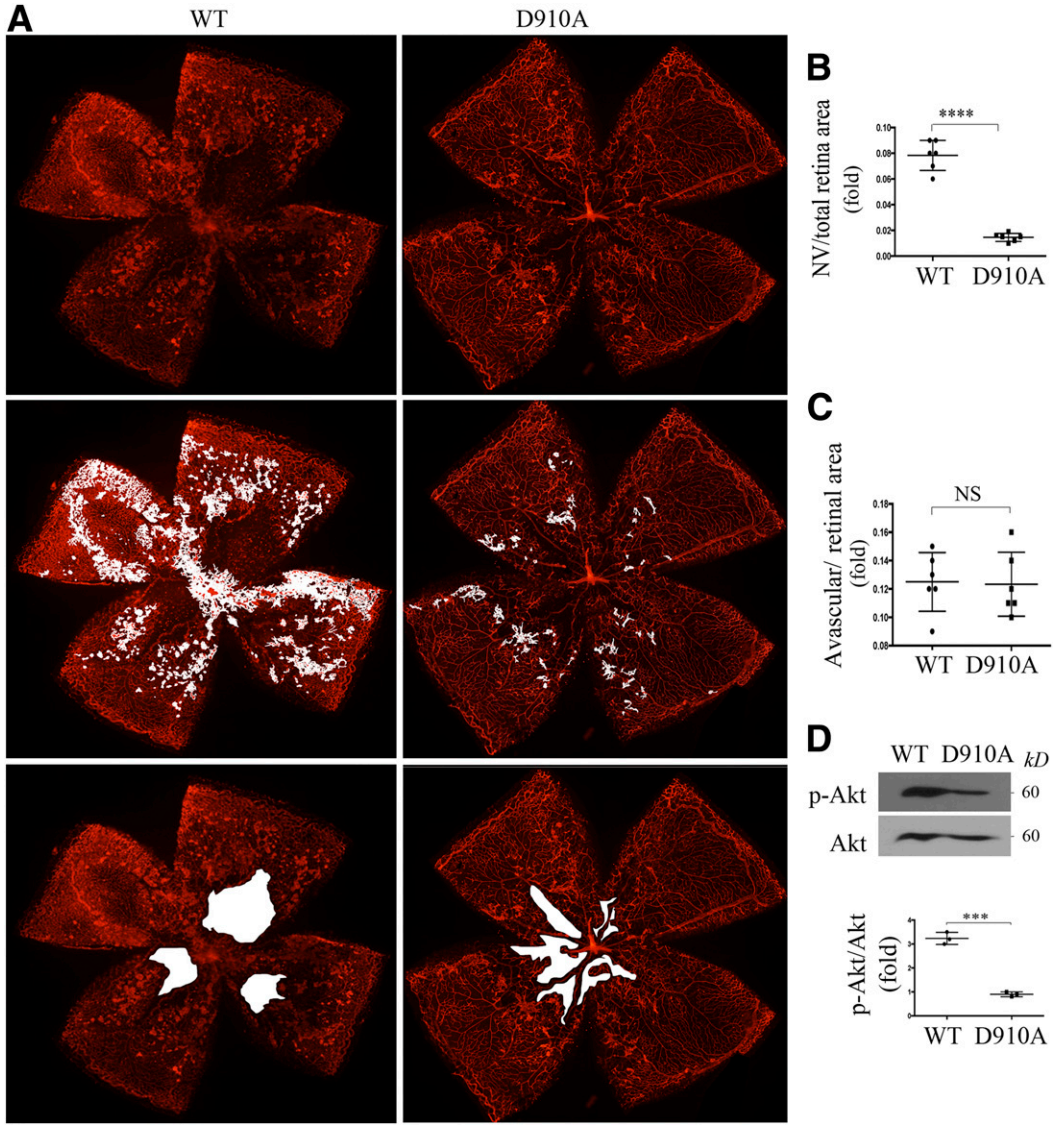

Figure 6— Genetic inactivation of p110δ attenuates Akt activation and aberrant angiogenesis in a mouse model of OIR. *A–C*: Litters of WT and p110δ$^{D910A/D910A}$ (D910A) mice were exposed to 75% oxygen for 5 days from P7 to P12 and then returned to room air. *A*: At P17, whole-mount retinas were stained with IB4 ($n = 6$). *B* and *C*: Analysis of pathological angiogenesis (tufts) and avascular areas from the IB4-stained retinas. ****$P < 0.0001$ between the two compared groups (six retinas/group) by unpaired *t* test. *D*: The clarified lysates of the retinas (one retina/lane) from P17 pups having experienced the OIR model were subjected to Western blot using the indicated antibodies. Data are mean ± SD of three independent experiments. ***$P < 0.001$ by unpaired *t* test. NV, neovascularization.

At P17, the whole-mount retinas from the euthanized pups were stained with IB4. Results showed a dramatic decrease in the number of preretinal tufts after treatment with idelalisib compared with vehicle (Fig. 8*A–C*). However, idelalisib did not arrest angiogenesis from the avascular area of retinas (Fig. 8*A–C*). In addition, idelalisib suppressed hypoxia-induced Akt activation in the P17 retinas (Fig. 8*D* and *E*). Taken together, these data show that inhibition of p110δ prevents hypoxia-induced Akt activation and pathological angiogenesis while sparing the central avascular area's revascularization in this mouse model of OIR. In summary, genetic (p110δ$^{D910A/D910A}$) or pharmacological (idelalisib) inactivation of p110δ in vivo demonstrates that p110δ plays an essential role in retinal pathological angiogenesis in OIR.

DISCUSSION

p110δ belongs to the receptor-regulated class IA PI3K lipid kinases, which also include the p110α and p110β isoforms. Whereas all class I PI3Ks couple to tyrosine kinase–linked receptors, p110β is also stimulated by G-protein–coupled receptors (12).

While TNF-α induces nuclear factor–κB)/p65–dependent expression of p110δ in HUVECs, our experimental

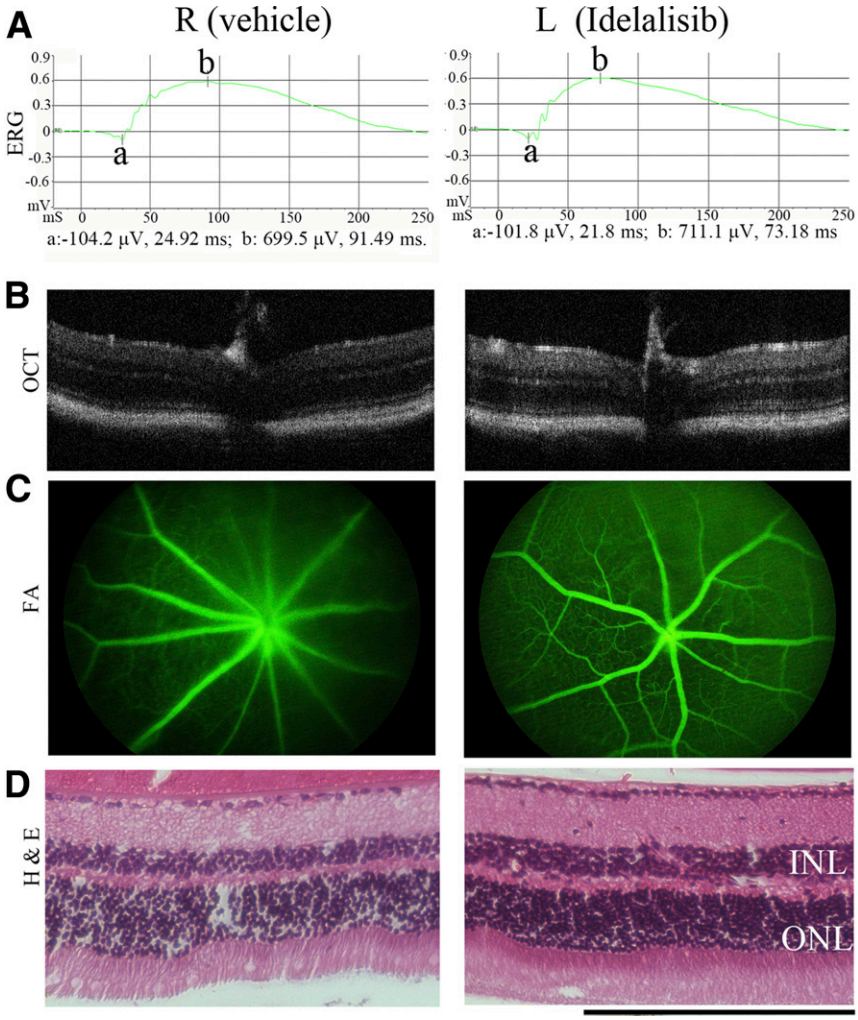

Figure 7—Evaluation of idelalisib toxicity to mouse eyes. Idelalisib was intravitreally injected into the mouse eyes on P12 to achieve a final vitreal concentration of ~10 μmol/L. This day was considered day 0. *A–D*: On day 30, the mouse eyes were examined by ERG (dark adaption), OCT, FFA, and histological analysis. Representative data are presented in each panel for the indicated analysis. Scale bar = 200 μm. H & E, hematoxylin and eosin; INL, inner nuclear layer; L, left eye; ONL, outer nuclear layer; R, right eye.

data revealed that high glucose enhances expression of p110δ in HRECs. We hypothesize that high glucose induces nuclear factor-κB/p65 activation (49), which promotes p110δ expression. Currently, we are actively testing this hypothesis .

Herein, we present our findings that VEGF, bFGF, and EGF are dependent on p110δ for activating Akt in HRECs. These findings demonstrate that p110δ can also transmit the signals from RTKs (e.g., VEGF receptor 2, EGF receptor, FGF receptor) to activate Akt in vascular ECs. This contrasts with a previous report that showed that in mouse cardiac ECs, p110α is a predominant isoform for activating of Akt (17). This difference might be due to a different cell type using a different PI3K isoform downstream of these RTKs. In addition, by using a mouse model of OIR, we found that p110δ is required for pathological angiogenesis but not central retinal revascularization, while p110α plays an essential role in developmental and tumor angiogenesis (50). The mechanism by which p110δ is required for pathological angiogenesis but not central retinal revascularization in the OIR mouse model and why the other PI3K isoforms fail to compensate when p110δ is antagonized warrant further investigation.

Of note, this OIR model is not actually a model of diabetic retinopathy because diabetic retinopathy is a complex disease that involves multiple genetic and environmental inputs (e.g., high glucose) (51). However, hypoxia in this OIR model induces pathological angiogenesis (preretinal tufts), which resemble the pathological neovascularization seen in human PDR. Therefore, this OIR model partially mimics the pathological angiogenesis in patients with PDR (46–48).

Idelalisib (also known as GS-1101, CAL-101, or Zydelig) is a selective inhibitor of p110δ approved by the U.S. Food

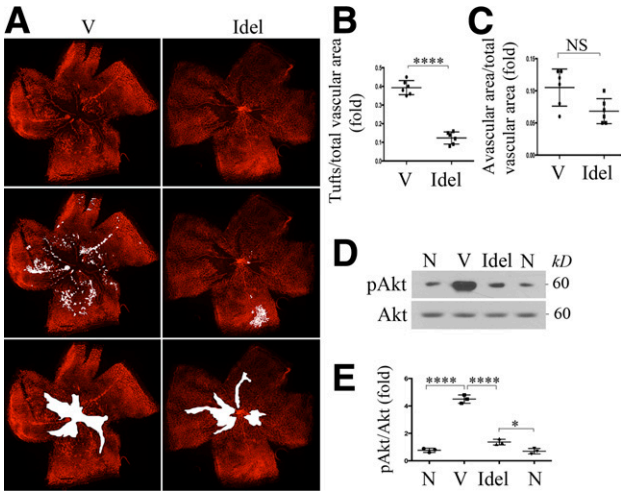

Figure 8—Inhibition of p110δ suppresses Akt activation and pathological angiogenesis in a mouse model of OIR. Litters of P12 mice that had been exposed to 75% oxygen for 5 days were injected intravitreally with idelalisib (Idel) (final vitreal concentration of ~10 μmol/L) or its vehicle (V) (0.1% DMSO) and then stayed in room air for 5 days. *A*: At P17, whole-mount retinas were stained with IB4. *B* and *C*: Analysis of neovascularization areas (tufts) from the IB4-stained retinas ($n = 6$) and avascular area ($n = 6$). *D* and *E*: Total lysates from retinas (one retina/lane) were subjected to Western blot analysis using the indicated antibodies. Data are mean ± SD of three independent experiments (folds). $^*P < 0.05$, $^{****}P < 0.0001$ between two compared groups by unpaired *t* test. N, retinas from P17 mice without experiencing 75% high oxygen.

and Drug Administration for the treatment of hematological malignancies (52). Our data provide a potentially alternative approach to treating patients with neovascular eye diseases who are not completely responsive to the current anti-VEGF treatment. Mainly because of its immunomodulatory effects, systemic exposure to idelalisib comes with warnings of possible toxicities that are serious and even fatal; the use of idelalisib to treat eyes might result in potential harmful side effects (53). However, this toxicity might not be observed upon intravitreal administration to treat angiogenesis-related eye diseases. With regard to the possible risk to the retina and visual function, our results show that a single intravitreal injection of idelalisib did not cause deleterious effects on retinal structure and function within 1 month (Fig. 7). However, if multiple intravitreal injections are needed to achieve suppression of pathological retinal neovascularization in clinical settings, retinal structure and function will have to be closely evaluated and monitored further.

In contrast to mice lacking p110α or p110β which show full or partial embryonic death (54,55), our experiments confirmed that mice with inactive p110δ are fertile and born at normal Mendelian ratios without gross anatomical or behavioral abnormalities (32), indicating that p110δ is not critical for development and physiological angiogenesis. However, our data clearly show that these mice display reduced pathological retinal angiogenesis in an OIR model (Fig. 6), demonstrating that p110δ activity contributes to pathological retinal angiogenesis. This is consistent with another report that p110δ inactivation does not affect normal vascular development (17). Because mice with inactive p110δ are viable, the other PI3K isoforms may replace p110δ activity during development and physiological angiogenesis, indicating that p110δ contributes exclusively to pathological retinal angiogenesis. Of note, leukocytes (e.g., macrophages), in which p110δ is highly expressed, also play an important role in angiogenesis (56), so whether p110δ plays an essential role in pathogenesis through ECs in vivo needs further investigation.

In conclusion, our findings establish a conceptual foundation for developing a p110δ-targeted approach to prevent and treat retinal angiogenesis such as that seen in PDR. Especially, the pharmacological (idelalisib) approach has great potential for development as an alternative for patients who suboptimally respond to current anti-VEGF drugs.

Acknowledgments. The authors thank Dr. Patricia A. D'Amore for revising the manuscript and Dr. Michele Leblanc (both from Schepens Eye Research Institute of Massachusetts Eye and Ear) for analysis of neovascularization in the whole-mount retinal staining. W.W. also wants to thank her mentor Professor Luosheng Tang (from Xiangya Hospital, Changsha, China) for advising on this project.

Funding. This work was supported by the China Scholarship Council (to W.W.); Central South University student innovation project 2016zzts148 (to W.W.), the National Eye Institute of the National Institutes of Health under award number R01-EY-012509 (to H.L.) and core grant P30-EY-003790, Global Ophthalmology Award Program (to H.L.); and Research to Prevent Blindness (to H.L.). W.W. is also supported by the National Natural Science Foundation of China (81900893) and the Science and Technology Plan Project of Hunan Province (2019RS2011).

No funding bodies had any role in study design, data collection and analysis, decision to publish, or preparation of the manuscript.

Duality of Interest. B.V. is a consultant for Karus Therapeutics (Oxford, U.K.), iOnctura (Geneva, Switzerland), and Venthera (Palo Alto, CA) and has received speaker fees from Gilead. There is a pending patent application related to this work (to H.L.) at Schepens Eye Research Institute of Massachusetts Eye and Ear. No other potential conflicts of interest relevant to this article were reported.

Author Contributions. W.W., G.Z., H.H., X.H., and H.J. performed the experiments and analyzed the results. S.M. provided reagents and critically revised the manuscript. A.K. conceived the experiments and revised the manuscript. J.C. and J.A.M. provided patient samples and revised the manuscript. B.V. provided reagents, helped to interpret the data, and edited the manuscript. X.X., J.W., and H.L. conceived the experiments and revised the manuscript. H.L. analyzed the data and wrote the manuscript. H.L. is the guarantor of this work and, as such, had full access to all the data in the study and takes responsibility for the integrity of the data and the accuracy of the data analysis.

References

1. Duh EJ, Sun JK, Stitt AW. Diabetic retinopathy: current understanding, mechanisms, and treatment strategies. JCI Insight 2017;2e93751

2. Williams R, Airey M, Baxter H, Forrester J, Kennedy-Martin T, Girach A. Epidemiology of diabetic retinopathy and macular oedema: a systematic review. Eye (Lond) 2004;18:963–983

3. Cross MJ, Claesson-Welsh L. FGF and VEGF function in angiogenesis: signalling pathways, biological responses and therapeutic inhibition. Trends Pharmacol Sci 2001;22:201–207

4. Ellis LM. Epidermal growth factor receptor in tumor angiogenesis. Hematol Oncol Clin North Am 2004;18:1007–1021, viii

5. Senger DR, Galli SJ, Dvorak AM, Perruzzi CA, Harvey VS, Dvorak HF. Tumor cells secrete a vascular permeability factor that promotes accumulation of ascites fluid. Science 1983;219:983–985
6. Mintz-Hittner HA, Kennedy KA, Chuang AZ; BEAT-ROP Cooperative Group. Efficacy of intravitreal bevacizumab for stage 3+ retinopathy of prematurity. N Engl J Med 2011;364:603–615
7. Chakravarthy U, Harding SP, Rogers CA, et al.; IVAN Study Investigators. Alternative treatments to inhibit VEGF in age-related choroidal neovascularisation: 2-year findings of the IVAN randomised controlled trial. Lancet 2013;382:1258–1267
8. Fogli S, Del Re M, Rofi E, Posarelli C, Figus M, Danesi R. Clinical pharmacology of intravitreal anti-VEGF drugs. Eye (Lond) 2018;32:1010–1020
9. Suzuki M, Nagai N, Izumi-Nagai K, et al. Predictive factors for non-response to intravitreal ranibizumab treatment in age-related macular degeneration. Br J Ophthalmol 2014;98:1186–1191
10. Vanhaesebroeck B, Stephens L, Hawkins P. PI3K signalling: the path to discovery and understanding. Nat Rev Mol Cell Biol 2012;13:195–203
11. Graupera M, Potente M. Regulation of angiogenesis by PI3K signaling networks. Exp Cell Res 2013;319:1348–1355
12. Bilanges B, Posor Y, Vanhaesebroeck B. PI3K isoforms in cell signalling and vesicle trafficking. Nat Rev Mol Cell Biol 2019;20:515–534
13. Vanhaesebroeck B, Welham MJ, Kotani K, et al. P110delta, a novel phosphoinositide 3-kinase in leukocytes. Proc Natl Acad Sci U S A 1997;94:4330–4335
14. Okkenhaug K. Signaling by the phosphoinositide 3-kinase family in immune cells. Annu Rev Immunol 2013;31:675–704
15. Ali K, Soond DR, Pineiro R, et al. Inactivation of PI(3)K p110δ breaks regulatory T-cell-mediated immune tolerance to cancer. Nature 2014;510:407–411
16. Chellappa S, Kushekhar K, Munthe LA, et al. The PI3K p110δ isoform inhibitor idelalisib preferentially inhibits human regulatory T cell function. J Immunol 2019;202:1397–1405
17. Graupera M, Guillermet-Guibert J, Foukas LC, et al. Angiogenesis selectively requires the p110alpha isoform of PI3K to control endothelial cell migration. Nature 2008;453:662–666
18. Haddad G, Zhabyeyev P, Farhan M, et al. Phosphoinositide 3-kinase β mediates microvascular endothelial repair of thrombotic microangiopathy. Blood 2014;124:2142–2149
19. Vanhaesebroeck B, Whitehead MA, Piñeiro R. Molecules in medicine mini-review: isoforms of PI3K in biology and disease. J Mol Med (Berl) 2016;94:5–11
20. Puri KD, Gold MR. Selective inhibitors of phosphoinositide 3-kinase delta: modulators of B-cell function with potential for treating autoimmune inflammatory diseases and B-cell malignancies. Front Immunol 2012;3:256
21. Bartok B, Hammaker D, Firestein GS. Phosphoinositide 3-kinase δ regulates migration and invasion of synoviocytes in rheumatoid arthritis. J Immunol 2014;192:2063–2070
22. Whitehead MA, Bombardieri M, Pitzalis C, Vanhaesebroeck B. Isoform-selective induction of human p110δ PI3K expression by TNFα: identification of a new and inducible PIK3CD promoter. Biochem J 2012;443:857–867
23. Huang X, Zhou G, Wu W, et al. Editing VEGFR2 blocks VEGF-induced activation of Akt and tube formation. Invest Ophthalmol Vis Sci 2017;58:1228–1236
24. Swiech L, Heidenreich M, Banerjee A, et al. In vivo interrogation of gene function in the mammalian brain using CRISPR-Cas9. Nat Biotechnol 2015;33:102–106
25. Sanjana NE, Shalem O, Zhang F. Improved vectors and genome-wide libraries for CRISPR screening. Nat Methods 2014;11:783–784
26. Lei H, Romeo G, Kazlauskas A. Heat shock protein 90alpha-dependent translocation of annexin II to the surface of endothelial cells modulates plasmin activity in the diabetic rat aorta. Circ Res 2004;94:902–909
27. Lei H, Qian CX, Lei J, Haddock LJ, Mukai S, Kazlauskas A. RasGAP promotes autophagy and thereby suppresses platelet-derived growth factor receptor-mediated signaling events, cellular responses, and pathology. Mol Cell Biol 2015;35:1673–1685
28. Tan E, Ding XQ, Saadi A, Agarwal N, Naash MI, Al-Ubaidi MR. Expression of cone-photoreceptor-specific antigens in a cell line derived from retinal tumors in transgenic mice. Invest Ophthalmol Vis Sci 2004;45:764–768
29. Lei H, Velez G, Hovland P, Hirose T, Gilbertson D, Kazlauskas A. Growth factors outside the PDGF family drive experimental PVR. Invest Ophthalmol Vis Sci 2009;50:3394–3403
30. Zhou G, Duan Y, Ma G, et al. Introduction of the MDM2 T309G mutation in primary human retinal epithelial cells enhances experimental proliferative vitreoretinopathy. Invest Ophthalmol Vis Sci 2017;58:5361–5367
31. Riss TL, Moravec RA, Niles AL, et al. Cell viability assays. In *Assay Guidance Manual*. Sittampalam GS, Coussens NP, Brimacombe K, et al., Eds. Bethesda, MD, Eli Lilly & Company and the National Center for Advancing Translational Sciences, 2004
32. Okkenhaug K, Bilancio A, Farjot G, et al. Impaired B and T cell antigen receptor signaling in p110delta PI 3-kinase mutant mice. Science 2002;297:1031–1034
33. Connor KM, Krah NM, Dennison RJ, et al. Quantification of oxygen-induced retinopathy in the mouse: a model of vessel loss, vessel regrowth and pathological angiogenesis. Nat Protoc 2009;4:1565–1573
34. Huang X, Zhou G, Wu W, et al. Genome editing abrogates angiogenesis in vivo. Nat Commun 2017;8:112
35. Longchamp A, Mirabella T, Arduini A, et al. Amino acid restriction triggers angiogenesis via GCN2/ATF4 regulation of VEGF and H2S production. Cell 2018;173:117–129.e14
36. Cui J, Lei H, Samad A, et al. PDGF receptors are activated in human epiretinal membranes. Exp Eye Res 2009;88:438–444
37. Lei H, Rheaume MA, Cui J, et al. A novel function of p53: a gatekeeper of retinal detachment. Am J Pathol 2012;181:866–874
38. Ma G, Duan Y, Huang X, et al. Prevention of proliferative vitreoretinopathy by suppression of phosphatidylinositol 5-phosphate 4-kinases. Invest Ophthalmol Vis Sci 2016;57:3935–3943
39. Puri KD, Doggett TA, Douangpanya J, et al. Mechanisms and implications of phosphoinositide 3-kinase delta in promoting neutrophil trafficking into inflamed tissue. Blood 2004;103:3448–3456
40. Tang J, Kern TS. Inflammation in diabetic retinopathy. Prog Retin Eye Res 2011;30:343–358
41. Rübsam A, Parikh S, Fort PE. Role of inflammation in diabetic retinopathy. Int J Mol Sci 2018;19942
42. Arnaoutova I, Kleinman HK. In vitro angiogenesis: endothelial cell tube formation on gelled basement membrane extract. Nat Protoc 2010;5:628–635
43. Gerber HP, McMurtrey A, Kowalski J, et al. Vascular endothelial growth factor regulates endothelial cell survival through the phosphatidylinositol 3′-kinase/Akt signal transduction pathway. Requirement for Flk-1/KDR activation. J Biol Chem 1998;273:30336–30343
44. Dimmeler S, Zeiher AM. Akt takes center stage in angiogenesis signaling. Circ Res 2000;86:4–5
45. Manning BD, Toker A. AKT/PKB signaling: navigating the network. Cell 2017;169:381–405
46. Chen J, Connor KM, Aderman CM, Willett KL, Aspegren OP, Smith LE. Suppression of retinal neovascularization by erythropoietin siRNA in a mouse model of proliferative retinopathy. Invest Ophthalmol Vis Sci 2009;50:1329–1335
47. Nagai N, Ju M, Izumi-Nagai K, et al. Novel CCR3 antagonists are effective mono- and combination inhibitors of choroidal neovascular growth and vascular permeability. Am J Pathol 2015;185:2534–2549
48. Stahl A, Connor KM, Sapieha P, et al. The mouse retina as an angiogenesis model. Invest Ophthalmol Vis Sci 2010;51:2813–2826
49. Ramana KV, Friedrich B, Srivastava S, Bhatnagar A, Srivastava SK. Activation of nuclear factor-kappaB by hyperglycemia in vascular smooth muscle cells is regulated by aldose reductase. Diabetes 2004;53:2910–2920

50. Soler A, Serra H, Pearce W, et al. Inhibition of the p110α isoform of PI 3-kinase stimulates nonfunctional tumor angiogenesis. J Exp Med 2013;210:1937–1945
51. Olivares AM, Althoff K, Chen GF, et al. Animal models of diabetic retinopathy. Curr Diab Rep 2017;17:93
52. Gopal AK, Kahl BS, de Vos S, et al. PI3Kδ inhibition by idelalisib in patients with relapsed indolent lymphoma. N Engl J Med 2014;370:1008–1018
53. Tang LA, Dixon BN, Maples KT, Poppiti KM, Peterson TJ. Current and investigational agents targeting the phosphoinositide 3-kinase pathway. Pharmacotherapy 2018;38:1058–1067
54. Foukas LC, Claret M, Pearce W, et al. Critical role for the p110alpha phosphoinositide-3-OH kinase in growth and metabolic regulation. Nature 2006; 441:366–370
55. Guillermet-Guibert J, Smith LB, Halet G, et al. Novel role for p110β PI 3-kinase in male fertility through regulation of androgen receptor activity in sertoli cells. PLoS Genet 2015;11:e1005304
56. Jetten N, Verbruggen S, Gijbels MJ, Post MJ, De Winther MP, Donners MM. Anti-inflammatory M2, but not pro-inflammatory M1 macrophages promote angiogenesis in vivo. Angiogenesis 2014;17:109–118